

# Optimization and calibration of atomic force microscopy sensitivity in terms of tip-sample interactions in high-order dynamic atomic force microscopy

Yu Liu,<sup>1</sup> Qiuquan Guo,<sup>2</sup> Heng-Yong Nie,<sup>3</sup> W. M. Lau,<sup>3</sup> and Jun Yang<sup>1,2,a)</sup>

<sup>1</sup>*Department of Mechanical and Materials Engineering, University of Western Ontario, London, Ontario N6A 5B9, Canada*

<sup>2</sup>*Biomedical Engineering Program, University of Western Ontario, London, Ontario N6A 5B9, Canada*

<sup>3</sup>*Surface Science Western, University of Western Ontario, London, Ontario N6A 5B7, Canada*

(Received 7 June 2009; accepted 4 November 2009; published online 28 December 2009)

The mechanism of dynamic force modes has been successfully applied to many atomic force microscopy (AFM) applications, such as tapping mode and phase imaging. The high-order flexural vibration modes are recent advancement of AFM dynamic force modes. AFM optical lever detection sensitivity plays a major role in dynamic force modes because it determines the accuracy in mapping surface morphology, distinguishing various tip-surface interactions, and measuring the strength of the tip-surface interactions. In this work, we have analyzed optimization and calibration of the optical lever detection sensitivity for an AFM cantilever-tip ensemble vibrating in high-order flexural modes and simultaneously experiencing a wide range and variety of tip-sample interactions. It is found that the optimal detection sensitivity depends on the vibration mode, the ratio of the force constant of tip-sample interactions to the cantilever stiffness, as well as the incident laser spot size and its location on the cantilever. It is also found that the optimal detection sensitivity is less dependent on the strength of tip-sample interactions for high-order flexural modes relative to the fundamental mode, i.e., tapping mode. When the force constant of tip-sample interactions significantly exceeds the cantilever stiffness, the optimal detection sensitivity occurs only when the laser spot locates at a certain distance from the cantilever-tip end. Thus, in addition to the “globally optimized detection sensitivity,” the “tip optimized detection sensitivity” is also determined. Finally, we have proposed a calibration method to determine the actual AFM detection sensitivity in high-order flexural vibration modes against the static end-load sensitivity that is obtained traditionally by measuring a force-distance curve on a hard substrate in the contact mode. © 2009 American Institute of Physics. [doi:10.1063/1.3269703]

## I. INTRODUCTION

The amplitude-modulated dynamic force modes in the operation of atomic force microscopy (AFM) commonly include the tapping mode, its secondary imaging mode, and the phase imaging mode. These modes of AFM have been widely applied to materials science and biological science due to their ability to probe not only the surface morphology but also the mechanical and chemical properties of materials with high spatial resolution.<sup>1,2</sup> In tapping mode, the cantilever/tip ensemble is excited at or close to its fundamental resonance frequency and the tip intermittently taps the sample surface with minimized destructive lateral forces.<sup>3</sup> While the oscillating tip approaches to or retracts from the sample surface under amplitude modulation, it experiences a complex and time-varying force field which contains a wealth of information about the materials composition,<sup>4</sup> electrical,<sup>5</sup> and mechanical properties,<sup>6</sup> as well as dissipative response of the sample.<sup>7,8</sup> As a result, such tip-sample interactions generate a disturbance to the vibration of the cantilever while it is tapping at the resonance frequency. Thus the motion of cantilever becomes anharmonic. In addition, the

effect of the tip-sample interactions often excites high-order flexural oscillation modes of the AFM cantilever.<sup>9,10</sup> Studies of these high-order oscillations are scientifically interesting and technologically important.

High-order dynamic force modes are recent advancements of AFM dynamic force microscopy, which further enhance AFM functionality in analyzing tip-sample interactions, surface composition, and material properties. Recently, researchers have investigated the possibility of using high-order flexural modes to explain the origins of the anharmonic spectra, and therefore extract the information of the tip-sample interactions. Such information cannot be obtained by the traditional dynamic analysis of tapping mode that is based on the fundamental resonance. Several recent studies of high-order dynamic force modes are highlighted as follows. Minne *et al.*<sup>11</sup> studied the second flexural mode to monitor the change in ZnO film admittance, which is not possible to probe while the AFM is operated at the fundamental resonance. Hoummady and Farnault<sup>12</sup> applied the second-order flexural mode to distinguish hydrodynamic damping and attractive interaction. They found that the AFM optical lever detection sensitivity was enhanced in the second-order flexural mode. Stark *et al.*<sup>9,13–15</sup> studied the origins of the increased anharmonic responses in high-order

<sup>a)</sup>Author to whom correspondence should be addressed. Electronic mail: jyang@eng.uwo.ca. Tel.: (519) 661 2111 ext. 80158. FAX: (519) 661 3020.

flexural modes due to nonlinear tip-sample interactions. They also resolved the force constants of the tip-sample interactions by analyzing a wide spectrum of flexural motions of the cantilever using the Fourier transformation. By simulating the AFM cantilever using finite element method, Song and Bhushan<sup>10</sup> studied the dynamic responses of the cantilever under both of attractive and repulsive force regimes, and concluded that the nonlinear force field excited high-order modes of the vertical bending. García's group<sup>16–18</sup> developed an approach to probe materials' properties by simultaneously exciting the first two flexural modes. The second-order flexural mode, generally a nonharmonic eigenmode of the cantilever,<sup>19</sup> is less coupled with the first-order mode according to the amplitude of vibration.<sup>16</sup> In their work, sample topography and composition contrast were obtained simultaneously through locking-in signals of the first two flexural modes, respectively. As a result, the sensitivity detected in the second-order flexural mode for compositional mapping was promoted by a factor of 10 because of a higher Q-factor. Further attempts were made by Sahin *et al.*<sup>20</sup> to enable a specially designed (notched) cantilever to reach the high-order harmonics of its high-order flexural modes. This consequently enables sensing the nonlinear mechanical interactions due to higher signal-to-noise ratio.<sup>21</sup>

In the study of the high-order flexural dynamics of AFM, the optical lever detection sensitivity, which is defined as the converting relationship between the measured AFM photodetector voltage and the cantilever deflection, plays a crucial role in determining the detectable minimum change of the vibrating amplitude. Since the minimum detectable force constant is proportional to the minimum detectable amplitude change,<sup>22</sup> a higher detection sensitivity is related to a better ability to detect a small force constant applied to the cantilever. In literature, studying and optimizing the optical lever detection sensitivity is an important issue not only for the design<sup>23</sup> but also for the operation of AFM systems such as for more accurate detection of tip-sample interactions.<sup>24,25</sup> Traditionally, the calibration of the detection sensitivity,  $\sigma_{FD}$ , of an optical lever AFM is done by measuring force-distance (FD) curves on a hard substrate in the contact mode.<sup>26</sup> The resultant detection sensitivity establishes a proportional relationship between the photodetector voltage output and the piezoelectric transducer displacement which is considered equal to the cantilever displacement deflection. In the tapping mode, this can be done through monitoring the voltage signal of the tapping amplitude attenuation relative to the tip-sample distance. However, researchers generally do not directly measure the displacement deflection of the cantilever.<sup>23,25,26</sup> For example, Butt and Jaschke<sup>27</sup> recognized that the cantilever deflection as measured by the scheme of optical lever detection was indeed the angular deflection of the cantilever, which is different from the actual displacement deflection of the cantilever as measured by an interferometer.<sup>26,28</sup> The angular change is dependent on the flexural modes of the cantilever. As a result, the FD curve method in the contact mode based on the condition of static end loading is not the best way to calibrate the detection sensitivity on a vibrating cantilever beam.<sup>25,29</sup> In fact, Walters *et al.*<sup>30</sup> pointed out that the optical lever detection

sensitivity in the first-order flexural mode should appear as a correction of  $\sigma_{FD}$  by a factor of 1.09 for a rectangular cantilever beam.

Furthermore, an infinitely small laser spot located at the tip end of the cantilever was assumed in previous studies.<sup>25</sup> Recently, researchers<sup>24,25,29,31,32</sup> have studied the effect of the size and the location of the laser spot that is focused on the cantilever backside, on the optical lever detection sensitivity in various cases. Our objective in this work is to discuss the theoretical optimum of the optical lever detection sensitivity in the high-order flexural vibration modes in common experimental conditions where a wide range of the force constant of tip-sample interactions may occur and therefore constrain the optimal operating condition of AFM systems. At the end, a useful calibration method will be demonstrated to correlate the sensitivity of tapping or a high-order flexural vibration mode with the traditional  $\sigma_{FD}$  when appropriate corrections apply.

## II. THEORY AND METHOD

### A. Flexural modes of a cantilever beam experiencing a force constant

A rectangular AFM cantilever beam can be modeled as a one-dimensional straight flexible beam made of homogeneous material and with a uniform cross section. With one end clamped at its base, the flexural dynamics of a rectangular cantilever beam is given by<sup>26,32,33</sup>

$$EI \frac{\partial^4 z(x,t)}{\partial x^4} + \rho A \frac{\partial^2 z(x,t)}{\partial t^2} = 0, \quad (1)$$

with the normalized coordinate  $x \in [0, 1]$  and time  $t$ . In Eq. (1),  $E$  is Young's modulus,  $\rho$  is the mass density,  $A$  is the cross section area,  $I$  is the area moment of inertia of the cantilever, and  $z(x,t)$  is the deflection of the cantilever as a function of position and time. For a freely vibrating cantilever, in its steady-state solution, the normalized shape function  $h_n(x)$  is<sup>34</sup>

$$h_n(x) = \frac{(-1)^n}{2} \left[ (\cos \kappa_n x - \cosh \kappa_n x) - \frac{(\cos \kappa_n + \cosh \kappa_n)}{(\sin \kappa_n + \sinh \kappa_n)} (\sin \kappa_n x - \sinh \kappa_n x) \right], \quad (2)$$

where  $n$  denotes the order of the flexural mode and  $\kappa_n$  is the dimensionless wave numbers which are determined by the characteristic equation,

$$\cos \kappa_n \cosh \kappa_n + 1 = 0. \quad (3)$$

It should be noted that Eq. (3) is for the beam with only one end clamped.

In the tapping mode, when the cantilever is engaged close to the sample surface by a separation distance  $d$ , it experiences nonlinear tip-sample interactions. However, if the cantilever vibrates with a very small amplitude around its equilibrium position  $d_0$ , the tip-sample force could be linearized as a spring with a force constant  $k_{\text{eff}} = -\partial F / \partial d|_{d=d_0}$ .<sup>35,36</sup> In this study,  $k_{\text{eff}}$  is the derivative of all tip-sample interaction

forces,  $F$ , with respect to the separation distance  $d$ . Consequently, a force  $k_{\text{eff}}z$  due to the deflection  $z$  should be added to the shear force,<sup>35</sup>

$$EI \frac{\partial^3 z}{\partial x^3} - k_{\text{eff}}z = 0, \quad (4)$$

with the following boundary conditions:

$$h_n(x) = 0 \quad \text{and} \quad \frac{\partial h_n(x)}{\partial x} = 0 \quad \text{at} \quad x = 0, \quad (5)$$

$$\frac{\partial^2 h_n(x)}{\partial x^2} = 0 \quad \text{and} \quad \frac{\partial^3 h_n(x)}{\partial x^3} = \frac{k_{\text{eff}}}{EI} h_n(x) = \frac{3k_{\text{eff}}}{k_C} h_n(x) \quad \text{at} \quad x = 1, \quad (6)$$

where  $k_C$  denotes the cantilever spring constant. To solve the characteristic equation for this system, the same procedure described in our previous study<sup>29</sup> is used to obtain

$$\begin{aligned} & \sinh \kappa_n \cos \kappa_n - \sin \kappa_n \cosh \kappa_n \\ &= \frac{(\kappa_n)^3 k_C}{3k_{\text{eff}}} (1 + \cos \kappa_n \cosh \kappa_n). \end{aligned} \quad (7)$$

If  $k_{\text{eff}}=0$ , Eq. (7) reduces to Eq. (3), which describes a freely vibrating cantilever. In the other extreme case when  $k_{\text{eff}}=\infty$ , the cantilever is pinned at both ends: base and tip. The dimensionless wave number  $\kappa_n$  is affected by the value of  $k_{\text{eff}}$  relative to the cantilever spring constant  $k_C$ . In this study, we only show the results for  $n$  up to 4 because we have found that the maximum detection sensitivity is nearly independent on the force constant if  $n \geq 4$  (results not shown here).

## B. Optical lever detection sensitivity

Previous studies have provided the expression of the optical lever detection sensitivity based on the classical diffraction theory.<sup>25,32,37,38</sup> In this paper, one-dimensional irradiation distribution of a Gaussian optical beam is assumed to perpendicularly impinge and be focused on the backside of the cantilever.<sup>25,38</sup> In addition, the effects of the torsion of the cantilever<sup>10,35</sup> and the interference from the sample are ignored in this paper. Therefore, we have

$$I(x) = \sqrt{\frac{8}{\pi}} \frac{P_0}{w_0} \exp\left(\frac{-8(x-\gamma)^2}{(w_0/L)^2}\right), \quad (8)$$

where  $P_0$  is the total power of the laser beam,  $w_0$  is the diameter of the Gaussian laser focused along the  $x$ -axis (longitudinal axis of the cantilever),  $L$  is the cantilever length, and  $\gamma$  is the relative location of the laser beam centered on the cantilever which is defined to be 0 at the base and 1 at the tip end.<sup>32</sup> As a result, the scalar wave function is

$$E(x) = \sqrt{\sqrt{\frac{8}{\pi}} \frac{P_0}{w_0}} \exp\left(\frac{-4(x-\gamma)^2}{(w_0/L)^2}\right). \quad (9)$$

The optical lever detection sensitivity at the  $n$ th order flexural mode is given as<sup>25,36</sup>

$$\sigma_n\left(\frac{w_0}{L}, \gamma\right) = \frac{4\alpha}{\lambda} \int_0^1 dx \int_0^1 dx' E(x)E(x') \frac{h_n(x) - h_n(x')}{x - x'}, \quad (10)$$

where  $\alpha$  denotes the loss factor when laser transmits from the laser source to the photodetector and  $\lambda$  is the laser wavelength. In the present work, we also assume no power loss ( $\alpha=1$ ).<sup>32</sup>

An “effective slope” of the section of the cantilever shined by the focused laser spot is given by<sup>24</sup>

$$\begin{aligned} c_n(\tau, \gamma) &= \frac{4}{\pi\tau^2} \int_0^1 dx \int_0^1 dx' E(x)E(x') \frac{h_n(x) - h_n(x')}{x - x'} \\ &\quad \times \exp\left[\frac{-4(x-\gamma)^2 - 4(x'-\gamma)^2}{\tau^2}\right], \end{aligned} \quad (11)$$

where  $\tau=w_0/L$  is the normalized spot size relative to the cantilever length. In optical lever deflection AFM,  $c_n(\tau, \gamma)$  is detected by the photodetector.

## III. RESULTS AND DISCUSSIONS

The absolute value of the optical lever detection sensitivity is proportional to the effective slope  $|c_n|$  by a constant. Thus we term  $|c_n|$  as the equivalent detection sensitivity in our discussion.<sup>24</sup> It is a function of both the normalized spot size  $\tau$  and the normalized location  $\gamma$ . The values of  $|c_n|$  for different ratios of  $k_{\text{eff}}/k_C$  are displayed as contour plots in Fig. 1, and Figs. 2–4 for the flexural modes at  $n=1, 2, 3$ , and 4, respectively. The maximum on the contour plot is defined to be the “globally optimized detection sensitivity”  $|c_{\text{global}}|$  of the optical lever AFM. When there are several local maxima on the contour plots, among them the local maximum closest to the cantilever-tip end is defined to be the “tip optimized detection sensitivity”  $|c_{\text{tip}}|$ .<sup>24</sup>

### A. Effect of $k_{\text{eff}}/k_C$ on detection sensitivity of tapping mode AFM

From Table I, for the first flexural mode ( $n=1$ ) or tapping mode, the globally optimized detection sensitivity  $|c_{\text{global}}|$  coincides with the tip optimized detection sensitivity  $|c_{\text{tip}}|$  at  $\tau \cong 0.95$  and  $\gamma \cong 0.57$  when  $k_{\text{eff}}/k_C < 1$ , as shown in Fig. 1(a). This is in agreement with the conclusion in Ref. 24: When the laser spot diameter is about 95% of the cantilever length and the spot center is located at about 57% away from the cantilever base, the optimum detection sensitivity for the first flexural mode of the optical lever AFM system can be attained. According to our study here, this conclusion should be constrained with another condition that  $k_{\text{eff}}/k_C$  may not significantly exceed 1. However, as shown in previous theoretical and experimental studies, a much higher  $k_{\text{eff}}/k_C$  is realistic and can go up to 200 or more.<sup>35,39,40</sup> Then the question remains: What if  $k_{\text{eff}}/k_C \gg 1$ ? We find, when  $k_{\text{eff}}/k_C$  significantly exceeds 1, the conditions for the globally optimized detection sensitivity may be changed. For example, when  $k_{\text{eff}}/k_C \gg 10$  in Table I, the normalized spot size decreases to  $\tau \cong 0.88$  and the normalized spot location shifts to  $\gamma \cong 0.43$ . This can be explained from Fig. 1(c) which describes the normalized spot locations where the absolute val-

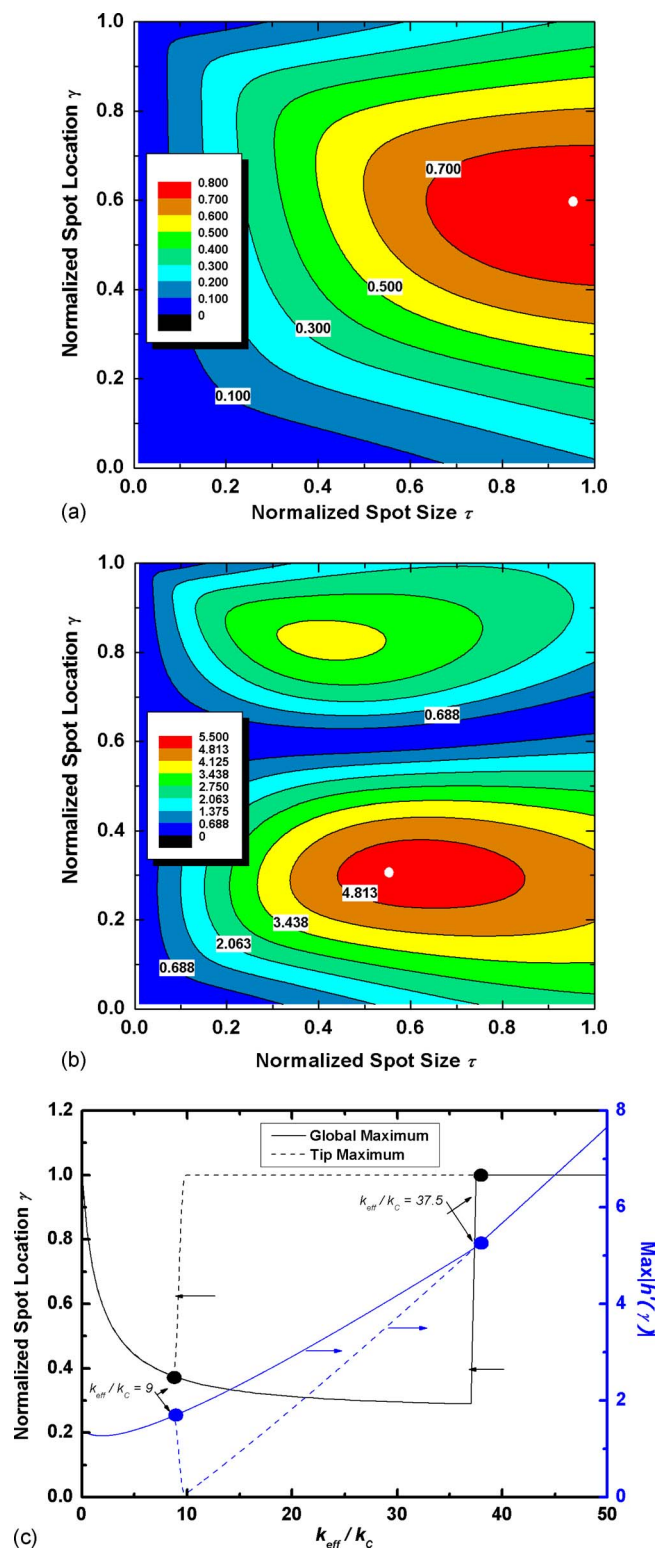


FIG. 1. (Color online) Contours of optical lever detection sensitivities in the first-order flexural mode plotted as function of normalized spot size  $\tau$  and normalized spot location  $\gamma$  for different ratios of the force constant to the spring constant of the cantilever: (a)  $k_{\text{eff}}/k_C=0.01$ ; (b)  $k_{\text{eff}}/k_C=100$ . The locations of the globally optimized detection sensitivity are shown as white dots “•” on the contours. (c) The normalized spot location  $\gamma$  and the cantilever slope  $|h'(\gamma)|$  for different  $k_{\text{eff}}/k_C$ .

ues of  $h'(\gamma)$ , the derivative of the shape function, are “global maximum” (black solid line) and “tip maximum” (black dashed line) for different values of  $k_{\text{eff}}/k_C$ . As mentioned before, the optical lever AFM systems detect the slope of the

cantilever rather than its displacement deflection. From Fig. 1(c), the normalized spot location  $\gamma$  of the global maximum  $|h'(\gamma)|$  ( $\max|h'(\gamma)|$ ) is shifted from the tip end to the cantilever base when  $k_{\text{eff}}/k_C$  is small or intermediate. As a result, the location of  $|c_{\text{global}}|$  is shifted.

If  $k_{\text{eff}}/k_C \gg 1$ , the globally optimized detection sensitivity and the tip optimized detection sensitivity tend to separate from each other. For example, when  $k_{\text{eff}}/k_C=100$  as shown in Fig. 1(b), for the globally optimized detection sensitivity,  $\tau_{\text{global}} \cong 0.55$  and  $\gamma_{\text{global}} \cong 0.31$ ; but for the tip optimized detection sensitivity,  $\tau_{\text{tip}} \cong 0.40$  and  $\gamma_{\text{tip}} \cong 0.85$ . This difference can also be partially explained in light of  $\max|h'(\gamma)|$ , which is directly related to the cantilever shape. When  $k_{\text{eff}}/k_C$  is relative small, tip maximum and global maximum for  $|h'(\gamma)|$  are identical to each other at the same spot location; but when  $k_{\text{eff}}/k_C$  becomes bigger, they become different. As a result, globally and tip optimized detection sensitivities become different as well. Figure 1(c) shows, according to Eq. (2), the separation point for the global maximum  $|h'(\gamma)|$  and the tip maximum  $|h'(\gamma)|$  is at  $k_{\text{eff}}/k_C=9$ . In the cantilever slope equation Eq. (2), it is assumed that the laser spot is zero-size point. In reality, the separation point for  $|c_{\text{global}}|$  and  $|c_{\text{tip}}|$  occurs at somewhere  $k_{\text{eff}}/k_C > 9$  since the size of the focused laser spot is not zero. Also as shown in Fig. 1(c), the global maximum  $|h'(\gamma)|$  and the tip maximum  $|h'(\gamma)|$  become identical to each other again after  $k_{\text{eff}}/k_C > 37.5$ . However such a crossover point for  $|c_{\text{global}}|$  and  $|c_{\text{tip}}|$  has not been obtained even when we increase  $k_{\text{eff}}/k_C$  up to a reasonably big value. This aberrance between  $\max|h'(\gamma)|$  and  $|c_{\text{global}}|$  is because the laser spot projecting on the cantilever backside is assumed as a point laser in the calculation of  $\max|h'(\gamma)|$ . Thus, using  $\max|h'(\gamma)|$  to predict the trend of optimized sensitivity is only valid for a certain range of the force constant  $k_{\text{eff}}$ . For higher  $k_{\text{eff}}/k_C$ , the finite size of the laser spot plays an important role in determining the optical detection sensitivity of the tapping mode AFM.

The globally optimized detection sensitivity  $|c_{\text{global}}|$  for tapping mode AFM at its resonance frequency is increased with the increase in  $k_{\text{eff}}/k_C$ . When  $k_{\text{eff}}/k_C=0$ ,  $|c_{\text{global}}| \cong 0.78$ ; when  $k_{\text{eff}}/k_C=100$ ,  $|c_{\text{global}}| \cong 5.22$ . The globally optimized detection sensitivity generally corresponds to the maximum value of  $|h'(\gamma)|$ . As shown in Fig. 1(c),  $\max|h'(\gamma)|$  monotonously increases as the increase in  $k_{\text{eff}}/k_C$ . Therefore, for a specific force constant  $k_{\text{eff}} = \partial F / \partial d$  such as a single molecule spring, using a softer cantilever with a smaller spring constant relative to the  $k_{\text{eff}} = \partial F / \partial d$  can enhance the detection sensitivity in order to obtain more accurate force measurement, and better phase contrast in phase imaging as well.<sup>41</sup> However, with a soft cantilever, hysteresis/bistability phenomena can be easily amplified.<sup>42,43</sup> In addition, the range of the “snap-to-contact” instability<sup>44</sup> encountered in the optical lever deflection AFM is enlarged, and the whole cantilever easily suffers from “jumping” or “snapping.”<sup>45,46</sup> Therefore, there is a necessity to make a tradeoff between  $k_C$  and  $k_{\text{eff}}$  to obtain the optimal result.

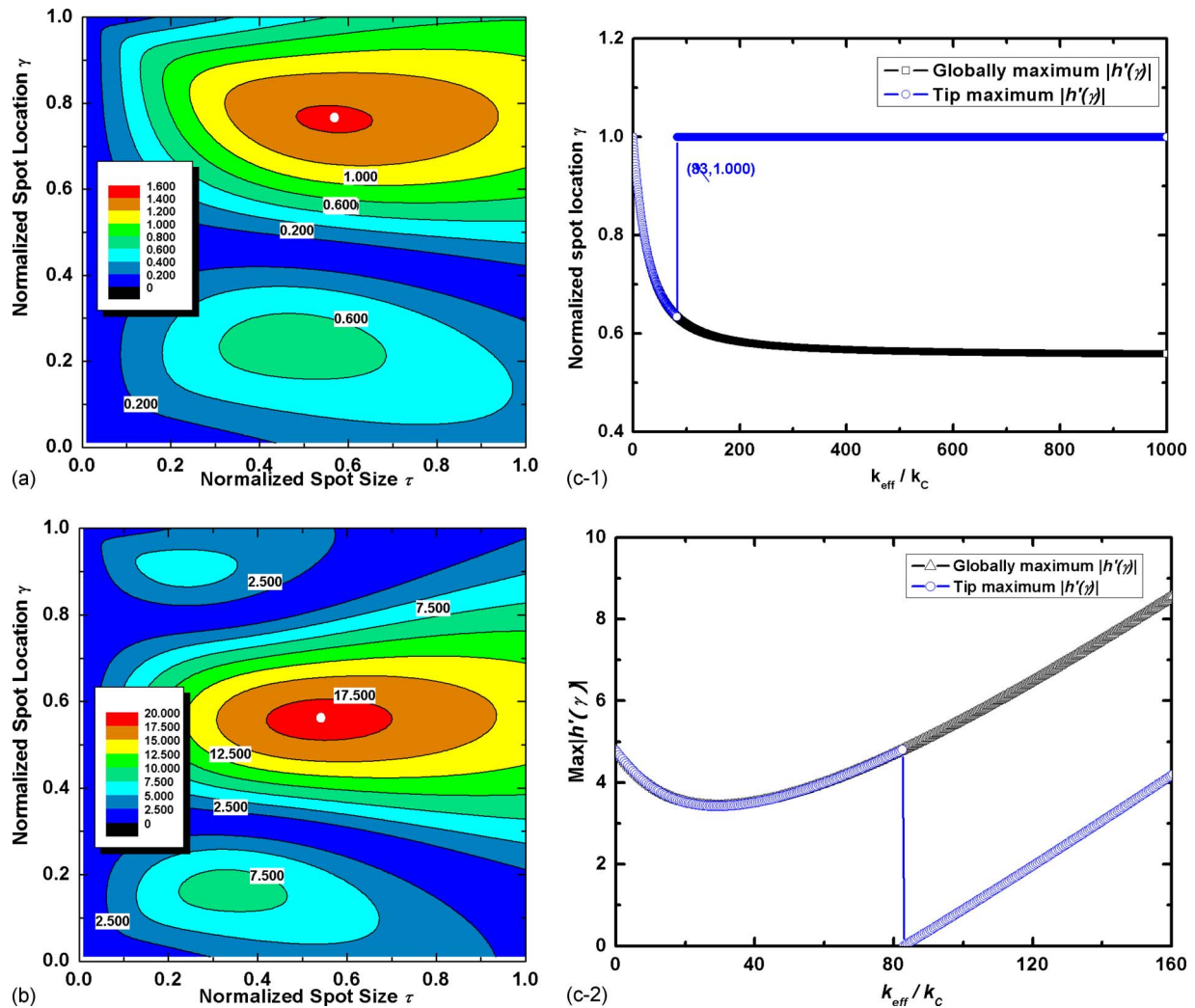


FIG. 2. (Color online) Contours of optical lever detection sensitivities in the second-order flexural mode plotted as function of normalized spot size  $\tau$  and normalized spot location  $\gamma$  for different ratios of the force constant to the spring constant of the cantilever: (a)  $k_{\text{eff}}/k_C=0.01$ ; (b)  $k_{\text{eff}}/k_C=1000$ . The locations of the globally optimized detection sensitivity are shown as white dots “ $\bullet$ ” on the contours. (c) Normalized spot location  $\gamma$  of globally and tip maximum values of  $|h'(\gamma)|$  for different  $k_{\text{eff}}/k_C$ .

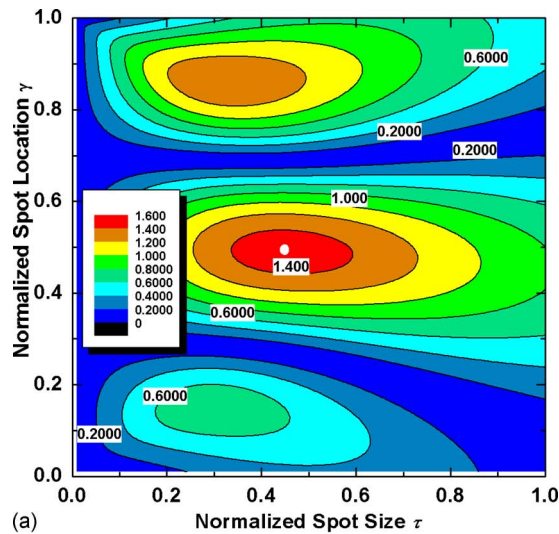
## B. Effect of $k_{\text{eff}}/k_C$ on the optical lever detection sensitivity in high-order flexural modes

High-order flexural dynamic modes of the AFM have attracted increasing interests from the AFM community.<sup>10-21</sup> For the second-order flexural mode, as shown in Fig. 2 and Table I, there are two local maxima for the cases of smaller  $k_{\text{eff}}/k_C$  and three local maxima for the case of  $k_{\text{eff}}/k_C = 1000$ . As  $k_{\text{eff}}/k_C$  increases, the location of the globally optimized detection sensitivity for the second-order flexural mode gradually shifts from the tip end to the base end of the cantilever, which is similar to what we have observed for the first flexural mode (tapping mode). For example, when  $k_{\text{eff}}/k_C = 10$ ,  $\gamma \approx 0.75$ ; when  $k_{\text{eff}}/k_C = 100$ ,  $\gamma \approx 0.63$ . For the second-order flexural mode, when  $k_{\text{eff}}/k_C = 1000$ , another local maximum appears close to the tip end of the cantilever, which is the tip optimized detection sensitivity. The reason is similar to what has been discussed for the case of the first-order flexural mode (tapping mode) in Sec. III A.

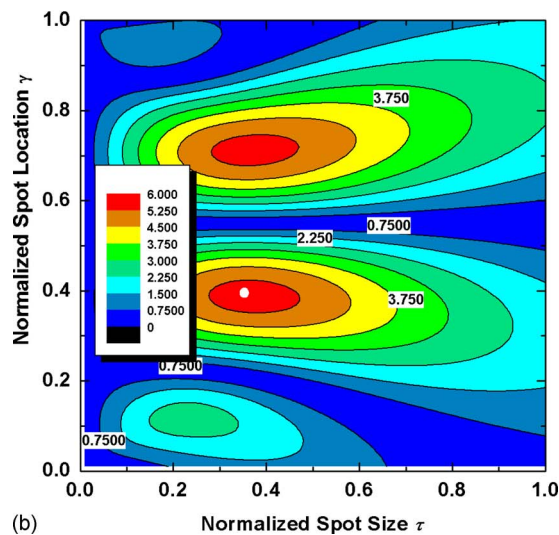
An additional local maximum is also found in the third- and fourth-order modes for large  $k_{\text{eff}}/k_C$ , as shown in Figs. 3 and 4. Higher-order ( $n > 4$ ) modes have also been examined,

whose results are not presented here since they are similar to those of the fourth-order mode. In contrast to the first and second-order flexural modes, the third- and fourth-order modes always have separate globally and tip optimized detection sensitivities for any value of  $k_{\text{eff}}/k_C$ , as shown in Figs. 3(a) and 4(a). As  $k_{\text{eff}}/k_C$  increases, both of tip and globally optimized sensitivities shift, as shown in Figs. 3(b) and 4(b). The additional local maximum, instead of the original tip optimized sensitivity, becomes the present  $|c_{\text{tip}}|$ .

The values of  $|c_{\text{global}}|$  and  $|c_{\text{tip}}|$  in Table I show that the high-order flexural modes are less affected by the increase in  $k_{\text{eff}}/k_C$ . For example, in the first-order flexural mode (tapping mode), the globally and tip optimized sensitivities for  $k_{\text{eff}}/k_C = 100$  are about eight and five times bigger than those for  $k_{\text{eff}}/k_C = 0.01$ , respectively. Such difference becomes much bigger for  $k_{\text{eff}}/k_C = 1000$  (we extend our theoretical study to this extreme case in order to cover the full range of the force constant encountered in reality; it is worth mentioning that  $k_{\text{eff}}/k_C$  at the order of 100 is realistic). However, for the second-order flexural mode, the differences are only about two times even for  $k_{\text{eff}}/k_C = 1000$ . In high-order modes,



(a)



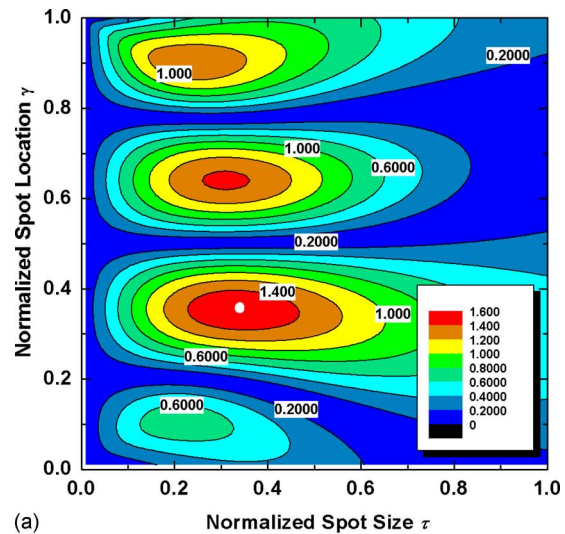
(b)

FIG. 3. (Color online) Contours of optical lever detection sensitivities in the third-order flexural mode plotted as function of normalized spot size  $\tau$  and normalized spot location  $\gamma$  for different ratios of the force constant to the spring constant of the cantilever: (a)  $k_{\text{eff}}/k_C=0.01$ ; (b)  $k_{\text{eff}}/k_C=1000$ . The locations of the globally optimized detection sensitivity are shown as white dots “•” on the contours.

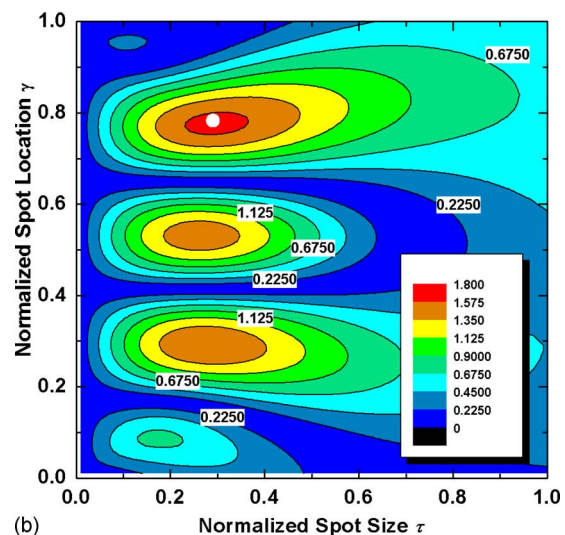
the detection sensitivities become almost independent on  $k_{\text{eff}}/k_C$  and only dependent on the spot size and location of the incident laser beam. This indicates that the optimized sensitivity values in high-order flexural modes become very reliable regardless of the variation of the force constant. This further leads to an important application: once the optimized sensitivity in high-order modes ( $n > 3$ ) is calibrated, the value can be used for working on any sample with trustable accuracy due to the reliability of the sensitivity, although the surface force field may change significantly from sample to sample.

### C. A practical calibration method for detection sensitivity of high-order flexural mode AFM

The optical lever detection sensitivity varies with many factors, such as laser alignment, cantilever backside coating, environmental medium, and optics and electronics of the AFM system. It is nearly impossible to calculate the correct



(a)



(b)

FIG. 4. (Color online) Contours of optical lever detection sensitivities in the fourth-order flexural mode plotted as function of normalized spot size  $\tau$  and normalized spot location  $\gamma$  for different ratios of the force constant to the spring constant of the cantilever: (a)  $k_{\text{eff}}/k_C=0.01$ ; (b)  $k_{\text{eff}}/k_C=10\,000$ . The locations of the globally optimized detection sensitivity are shown as white dots “•” on the contours.

detection sensitivity based on the limited information of specifications provided by manufacturers. Therefore, the detection sensitivity for an optical lever AFM is generally implemented by measuring FD curves on a hard substrate, which generates an approximately linear relationship between the output voltage of the photodetector and the deflection of the cantilever with a unit of mV/nm.

In the FD curve method, the deflection of the cantilever arises from a static loading at its tip end and the normalized cantilever shape function is<sup>25</sup>

$$h_0(x) = \frac{3x^2 - x^3}{2}. \quad (12)$$

Substituting Eq. (12) into Eq. (11), we plot the optical lever detection sensitivity as a function of the normalized spot location and size, as shown in Fig. 5. In this method, the corresponding globally optimized sensitivity is 0.778 at  $\tau \cong 0.94$  and  $\gamma \cong 0.58$ , which is the same as the tip optimized

TABLE I. Normalized spot size and location of the globally optimized sensitivity and the tip optimized sensitivity as a function of  $k_{\text{eff}}/k_C$ .

Mode No.	$k_{\text{eff}}/k_C$	Globally optimized			Tip optimized		
		$\tau_{\text{global}}$	$\gamma_{\text{global}}$	$ c_{\text{global}} $	$\tau_{\text{tip}}$	$\gamma_{\text{tip}}$	$ c_{\text{tip}} $
$n=1$	0	0.952	0.569	0.783	0.952	0.569	0.783
	0.01	0.951	0.569	0.783	0.951	0.569	0.783
	0.1	0.952	0.567	0.784	0.952	0.567	0.784
	1	0.957	0.554	0.790	0.957	0.554	0.790
	10	0.881	0.430	0.939	0.881	0.430	0.939
	100	0.553	0.305	5.165	0.400	0.850	3.571
	1000	0.580	0.280	51.797	0.430	0.810	43.346
$n=2$	0	0.562	0.763	1.421	0.562	0.763	1.421
	0.01	0.562	0.763	1.420	0.562	0.763	1.420
	0.1	0.563	0.763	1.419	0.563	0.763	1.419
	1	0.566	0.761	1.405	0.566	0.761	1.405
	10	0.595	0.745	1.317	0.595	0.745	1.317
	100	0.635	0.627	2.022	0.635	0.627	2.022
	1000	0.540	0.560	18.342	0.220	0.910	5.935
$n=3$	0	0.453	0.490	1.501	0.325	0.862	1.368
	0.01	0.453	0.490	1.501	0.325	0.862	1.368
	0.1	0.453	0.490	1.500	0.325	0.862	1.368
	1	0.452	0.490	1.492	0.325	0.862	1.365
	10	0.449	0.486	1.413	0.331	0.859	1.340
	100	0.390	0.830	1.271	0.390	0.830	1.271
	1000	0.370	0.390	5.583	0.370	0.710	5.537
$n=4$	0	0.335	0.353	1.560	0.233	0.901	1.371
	0.01	0.335	0.353	1.560	0.233	0.901	1.371
	0.1	0.335	0.353	1.560	0.233	0.901	1.371
	1	0.335	0.353	1.560	0.233	0.901	1.372
	10	0.334	0.352	1.560	0.234	0.900	1.383
	100	0.327	0.345	1.560	0.250	0.891	1.500
	10 000	0.290	0.780	1.640	0.290	0.780	1.640
50 000	0.290	0.770	1.636	0.290	0.770	1.636	

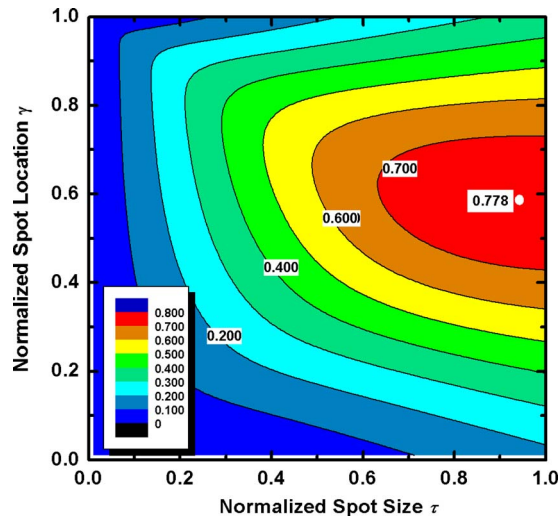


FIG. 5. (Color online) Contour of optical lever detection sensitivity of the static end-loading cantilever (FD curve mode) plotted as a function of the normalized spot size  $\tau$  and the normalized location  $\gamma$ . The globally optimized and tip optimized sensitivities are identical to each other as marked by a white dot “ $\circ$ .”

sensitivity. The method of static end-loading FD curve has nothing to do with the force constant that however plays a major role in dynamic force modes. Herein, we propose a simple calibration method to determine the optical lever detection sensitivity in high-order flexural modes with an important premise that  $k_{\text{eff}}/k_C < 1$ . This premise should be, and can be easily, satisfied before starting an AFM experiment through choosing an AFM cantilever with an appropriate spring constant.

To explain the method, we utilize Eqs. (4) and (5) from the works by Schäffer and Fuchs,<sup>24</sup>

$$\sigma_n(\tau, \gamma) = \sigma_0 c_n(\tau, \gamma) \quad (13)$$

and

$$\sigma_0 = \sqrt{\frac{\pi 4 P_0 \alpha(\tau, \gamma)}{4 \lambda}} D, \quad (14)$$

where  $P_0$  is the laser power and  $D$  is a constant related to the title angle of the cantilever.

Considering the power loss during laser transmission, the power received by the photodetector is  $P_0 \alpha(\tau, \gamma)$ . In practice, it is difficult to find out  $\alpha(\tau, \gamma)$  due to varying ex-

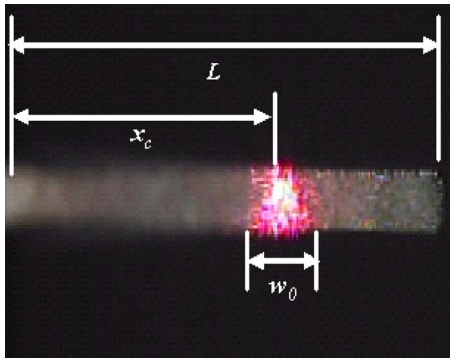


FIG. 6. (Color online) Focused laser spot on the cantilever backside with the normalized spot size  $\tau=0.16$  and normalized spot location  $\gamma=0.59$ . The length of the cantilever  $L$  is  $230\ \mu\text{m}$ .

perimental conditions. For operation of a well-structured AFM in air, there is less power loss related to the optical lens and transmission medium (it should be noted that for operation in liquid, the liquid medium causes more power loss<sup>32</sup>). Most part of  $\alpha(\tau, \gamma)$  results from the misalignment of the cantilever on its holder and the nonuniformity of the cantilever backside coating.  $\alpha(\tau, \gamma)$  is typically a function of the spot size and location. We need to determine both  $\tau$  and  $\gamma$  according to the method described below.

As shown in Fig. 6, a cantilever with a length of  $230\ \mu\text{m}$  was visualized under a top-view charge coupled device camera of our AFM system. We captured the image of the whole cantilever with a laser spot on it. A good alignment in our operation ensured that the aspect ratio of the laser spot was close to 1 (i.e., a nearly circular spot). The laser spot, as shown in Fig. 6, wholly falls on the cantilever. As a result, there is no significant light power spilled over the lateral edge of the cantilever.<sup>25</sup> Such a good alignment can also help eliminate the effects of the interference from the sample and the stray light. The normalized spot size and location are  $\tau \cong 0.16$  and  $\gamma \cong 0.59$ , respectively. Correspondingly, the effective slope is  $|c_0| \cong 0.22$ . For a commercial AFM, the user has no access to adjusting the focused spot size on the cantilever. However, using a homebuilt tunable slit aperture,<sup>25</sup> one can obtain  $\tau \cong 0.94$ . In addition, one can use a shorter cantilever in order to enlarge  $\tau$  to an extent. In this study,  $\tau \cong 0.16$  limits our ability to find the globally optimized detection sensitivity. Hence we can only fine tune the spot location.

Subsequently, the slope of the FD curve in Fig. 7 for this cantilever-laser spot ensemble was used to determine the sensitivity of the cantilever with static end loading,  $\sigma_{\text{FD}}$ , which was equal to  $41.5\ \text{mV/nm}$ . Based on Eq. (13), the corresponding  $\sigma_0$  is  $\sigma_{\text{FD}}/|c_0| \cong 188.6\ \text{mV/nm}$ . From Eq. (11), we also have the value of the effective slope of the cantilever in high-order flexural modes when  $\tau \cong 0.16$  and  $\gamma \cong 0.59$ :  $|c_1| \cong 0.20$ ,  $|c_2| \cong 0.30$ ,  $|c_3| \cong 0.61$ , and  $|c_4| \cong 0.90$ . Therefore, the detection sensitivities in the high-order flexural modes are  $\sigma_1 \cong 37.7\ \text{mV/nm}$ ,  $\sigma_2 \cong 56.6\ \text{mV/nm}$ ,  $\sigma_3 \cong 115.0\ \text{mV/nm}$ , and  $\sigma_4 \cong 169.7\ \text{mV/nm}$ , respectively. The results demonstrate that the higher order of the flexural vibration mode, the larger detection sensitivity, which is in good agreement with previous works (e.g., Refs. 12–14). As

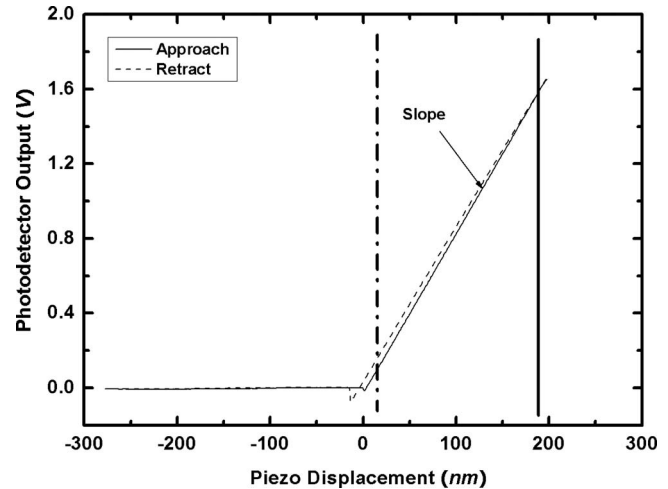


FIG. 7. A FD curve obtained in contact mode AFM. The slope of the loading portion of this FD curve is used to determine the sensitivity of the static end-loading cantilever, which is further used to demonstrate the calibration method for detection sensitivity in the high-order flexural vibration modes.

we mentioned earlier in this article, in order to adopt this calibration method, a cantilever having a spring constant larger than the force constant should be chosen for AFM experiments. This is indeed consistent with the practice for tapping mode where a stiff cantilever is preferred in order to avoid instability caused by a rather large attractive force constant during operation, which may amount to  $10\ \text{N/m}$  or more<sup>40</sup> for many samples.

#### IV. CONCLUSION

For dynamic force microscopy applications of an optical lever AFM system, the optimal detection sensitivity is determined in this study as a function of the order of the flexural vibration mode, the ratio of the force constant to the cantilever stiffness ( $k_{\text{eff}}/k_C$ ), the laser spot size, and location on the cantilever. We have tabulated a chart of the globally optimized detection sensitivity and the tip optimized detection sensitivity in the fundamental and high-order flexural modes for different  $k_{\text{eff}}/k_C$ . The optimized sensitivities in high-order flexural modes are less affected by  $k_{\text{eff}}/k_C$ . They are more stable than that of the fundamental mode (e.g., tapping mode). For  $k_{\text{eff}}/k_C < 1$ , we have developed a calibration method for the detection sensitivity in high-order modes. Our results show that the detection sensitivity is not only more stable but is also largely enhanced in high-order flexural modes.

#### ACKNOWLEDGMENTS

The authors are grateful for the financial support from the Natural Science and Engineering Research Council of Canada (NSERC), Canadian Institutes of Health Research (CIHR), Ontario Centers of Excellence (OCE), LANXESS Inc., and Shared Hierarchical Academic Research Computing Network (SHARCNET). Y.L. is grateful for the fellowship support from the Ontario Graduate Scholarship Program.

- <sup>1</sup>Q. Zhong, D. Inniss, K. Kjoller, and V. B. Elings, *Surf. Sci.* **290**, L688 (1993).
- <sup>2</sup>Y. K. Jiao and T. E. Schaffer, *Langmuir* **20**, 10038 (2004).
- <sup>3</sup>N. A. Burnham, O. P. Behrend, F. Oulevey, G. Gremaud, P. J. Gallo, D. Gourdon, E. Dupas, A. J. Kulik, H. M. Pollock, and G. A. D. Briggs, *Nanotechnology* **8**, 67 (1997).
- <sup>4</sup>R. Höper, T. Gesang, W. Possart, O. D. Hennemann, and S. Boseck, *Ultramicroscopy* **60**, 17 (1995).
- <sup>5</sup>U. Bostanci, M. K. Abak, O. Aktas, and A. Dâna, *Appl. Phys. Lett.* **92**, 093108 (2008).
- <sup>6</sup>J. Tamayo and R. García, *Appl. Phys. Lett.* **71**, 2394 (1997).
- <sup>7</sup>J. P. Cleveland, B. Anczykowski, A. E. Schmid, and V. B. Elings, *Appl. Phys. Lett.* **72**, 2613 (1998).
- <sup>8</sup>R. García, J. Tamayo, and A. S. Paulo, *Surf. Interface Anal.* **27**, 312 (1999).
- <sup>9</sup>R. Hillenbrand, M. Stark, and R. Guckenberger, *Appl. Phys. Lett.* **76**, 3478 (2000).
- <sup>10</sup>Y. X. Song and B. Bhushan, *Ultramicroscopy* **106**, 847 (2006).
- <sup>11</sup>S. C. Minne, S. R. Manalis, A. Atalar, and C. F. Quate, *Appl. Phys. Lett.* **68**, 1427 (1996).
- <sup>12</sup>M. Hoummady and E. Farnault, *Appl. Phys. A: Mater. Sci. Process.* **66**, S361 (1998).
- <sup>13</sup>R. W. Stark and W. M. Heckl, *Surf. Sci.* **457**, 219 (2000).
- <sup>14</sup>M. Stark, R. W. Stark, W. M. Heckl, and R. Guckenberger, *Proc. Natl. Acad. Sci. U.S.A.* **99**, 8473 (2002).
- <sup>15</sup>R. W. Stark and W. M. Heckl, *Rev. Sci. Instrum.* **74**, 5111 (2003).
- <sup>16</sup>T. R. Rodríguez and R. García, *Appl. Phys. Lett.* **84**, 449 (2004).
- <sup>17</sup>N. F. Martínez, S. Patil, J. R. Lozano, and R. García, *Appl. Phys. Lett.* **89**, 153115 (2006).
- <sup>18</sup>J. R. Lozano and R. García, *Phys. Rev. B* **79**, 014110 (2009).
- <sup>19</sup>R. Proksch, *Appl. Phys. Lett.* **89**, 113121 (2006).
- <sup>20</sup>O. Sahin, G. Yaralioglu, R. Grow, S. F. Zappe, A. Atalar, C. Quate, and O. Solgaard, *Sens. Actuators, A* **114**, 183 (2004).
- <sup>21</sup>O. Sahin, C. F. Quate, O. Solgaard, and A. Atalar, *Phys. Rev. B* **69**, 165416 (2004).
- <sup>22</sup>Y. Martin, C. C. Williams, and H. K. Wickramasinghe, *J. Appl. Phys.* **61**, 4723 (1987).
- <sup>23</sup>L. Y. Beaulieu, M. Godin, O. Laroche, V. Tabard-Cossa, and P. Grütter, *Appl. Phys. Lett.* **88**, 083108 (2006).
- <sup>24</sup>T. E. Schäffer and H. Fuchs, *J. Appl. Phys.* **97**, 083524 (2005).
- <sup>25</sup>T. E. Schäffer and P. K. Hansma, *J. Appl. Phys.* **84**, 4661 (1998).
- <sup>26</sup>D. Sarid, *Scanning Force Microscopy with Applications to Electric, Magnetic and Atomic Forces* (Oxford University Press, Oxford, 1994).
- <sup>27</sup>H. J. Butt and M. Jascheke, *Nanotechnology* **6**, 1 (1995).
- <sup>28</sup>D. Rugar, H. J. Mamin, R. Erlandsson, J. E. Stern, and B. D. Terris, *Rev. Sci. Instrum.* **59**, 2337 (1988).
- <sup>29</sup>S. Naeem, Y. Liu, H.-Y. Nie, W. M. Lau, and J. Yang, *J. Appl. Phys.* **104**, 114504 (2008).
- <sup>30</sup>D. A. Walters, J. P. Cleveland, N. H. Thomson, P. K. Hansma, M. A. Wendman, G. Gurley, and V. Erlings, *Rev. Sci. Instrum.* **67**, 3583 (1996).
- <sup>31</sup>R. Proksch, T. E. Schäffer, J. P. Cleveland, R. C. Callahan, and M. B. Viani, *Nanotechnology* **15**, 1344 (2004).
- <sup>32</sup>Y. Liu and J. Yang, *Nanotechnology* **19**, 235501 (2008).
- <sup>33</sup>U. Rabe, S. Hirsekorn, M. Reinstädler, T. Sulzbach, Ch. Lehrer, and W. Arnold, *Nanotechnology* **18**, 044008 (2007).
- <sup>34</sup>S. Timoshenko, *Vibration Problems in Engineering*, 4th ed. (Wiley, New York, 1974).
- <sup>35</sup>U. Rabe, K. Janser, and W. Arnold, *Rev. Sci. Instrum.* **67**, 3281 (1996).
- <sup>36</sup>J. A. Turner and J. S. Wiehn, *Nanotechnology* **12**, 322 (2001).
- <sup>37</sup>R. W. Stark, *Rev. Sci. Instrum.* **75**, 5053 (2004).
- <sup>38</sup>E. Hecht, *Optics*, 4th ed. (Addison-Wesley, Readings, MA, 2002).
- <sup>39</sup>U. Rabe, J. Turner, and W. Arnold, *Appl. Phys. A: Mater. Sci. Process.* **66**, S277 (1998).
- <sup>40</sup>F. J. Giessibl, *Rev. Mod. Phys.* **75**, 949 (2003).
- <sup>41</sup>X. Chen, M. C. Davies, C. J. Roberts, S. J. B. Tendler, P. M. Williams, and N. A. Burnham, *Surf. Sci.* **460**, 292 (2000).
- <sup>42</sup>R. Boisgard, D. Michel, and J. P. Aimé, *Surf. Sci.* **401**, 199 (1998).
- <sup>43</sup>Y. Sugawara, N. Kobayashi, M. Kawakami, Y. J. Li, Y. Naitoh, and M. Kageshima, *Appl. Phys. Lett.* **90**, 194104 (2007).
- <sup>44</sup>O. L. Warren, J. F. Graham, and P. R. Norton, *Rev. Sci. Instrum.* **68**, 4124 (1997).
- <sup>45</sup>S. A. Joyce and J. E. Houston, *Rev. Sci. Instrum.* **62**, 710 (1991).
- <sup>46</sup>N. Kato, I. Suzuki, H. Kikuta and K. Iwata, *Rev. Sci. Instrum.* **66**, 5532 (1995).